A Journal of the Gesellschaft Deutscher Chemiker

Angewandte International Edition GDCh Chemie

www.angewandte.org

Accepted Article

Title: Reversible Self-Assembly of N-Heterocyclic Carbene on Metal Surfaces

Authors: Jindong Ren, Matthias Freitag, Yuxiang Gao, Peter Bellotti, Mowpriya Das, Bertram Schulze Lammers, Harry Mönig, Yuyang Zhang, Constantin G. Daniliuc, Shixuan Du, Harald Fuchs, and Frank Glorius

To be cited as: *Angew. Chem. Int. Ed.* **2022**, e202115104

Link to VoR: https://doi.org/10.1002/anie.202115104

WILEY-VCH

10.1002/anie.202115104

WILEY-VCH

Reversible Self-Assembly of N-Heterocyclic Carbene on Metal Surfaces

Jindong Ren[a,b,c]‡, Matthias Freitag[d]‡, Yuxiang Gao[f]‡, Peter Bellotti[d], Mowpriya Das[d], Bertram Schulze Lammers[b,c], Harry Mönig[b,c], Yuyang Zhang[f], Constantin G. Daniliuc[d], Shixuan Du[f,g]*, Harald Fuchs[b,c,e]*, and Frank Glorius[d]*

[a] J. Ren
CAS Key Laboratory of Nanophotonic Materials and Devices, CAS Key Laboratory of Standardization and Measurement for Nano-technology, National Center for Nanoscience and Technology, Beijing 100190, P.R. China
[b] J. Ren, B.Schulze Lammers, H. Mönig, H. Fuchs*
Physikalisches Institut, Westfälische Wilhelms-Universität, Wilhelm-Klemm-Straße 10, Münster 48149, Germany. Email: fuchsh@uni-muenster.de
[c] J. Ren, B. Schulze Lammers, H. Mönig, H. Fuchs*
Center for Nanotechnology, Heisenbergstraße 11, Münster 48149, Germany.
[d] M. Freitag, P. Bellotti, M. Das, F. Glorius*
Organisch-Chemisches Institut, Westfälische Wilhelms-Universität, Corrensstraße 40, Münster 48149, Germany. Email: glorius@uni-muenster.de
[e] H. Fuchs
Herbert Gleiter Institute of Nanoscience, Nanjing University of Science and Technology, Nanjing 210094, P. R. China.
[f] Y. Gao, Y. Zhang, S. Du*
Institute of Physics and University of Chinese Academy of Sciences, Chinese Academy of Sciences, Beijing 100190, P.R. China. Email: sxdu@iphy.ac.cn
[g] S. Du
Songshan Lake Materials Laboratory, Dongguan, Guangdong 523808, P.R. China.

‡ These authors contributed equally

Abstract: Self-assembly of cyclohexyl cyclic (alkyl)(amino)carbenes (cyCAAC) can be realized and reversibly switched from a close-packed trimer phase to a chainlike dimer phase, enabled by the ring-flip of the cyclohexyl wingtip. Multiple methods including scanning tunneling microscopy (STM), X-ray photoelectron spectroscopy (XPS) and density functional theory (DFT) calculations identified a distinct isomer (axial or equatorial chair conformer) in each phase, and consequently support the conclusion regarding the determination of molecular surface geometry on the self-assembly of cyCAAC. Moreover, various substrates such as Ag (111) and Cu (111) are tested to elucidate the importance of cyCAAC-surface interactions on cyCAAC based nanopatterns. These investigations of patterned surfaces prompted a deep understanding of cyCAAC binding mode, surface geometry and reversible self-assembly, which are of paramount significance in the areas of catalysis, biosensor design and surface functionalization.

Introduction

Since the seminal report by Arduengo *et al.*,[1] N-heterocyclic carbenes (NHCs) have fostered considerable interest in catalysis,[2–4] as ligands for p-block elements[5] and transition metals,[6] thanks to their unique properties.[7,8] Owing to the strong σ-donating ability and the high tunability of the side-groups, manifold applications dealing with the functionalization of surfaces[9–13] and nanoparticles[14–21] have been reported.[22–24] The even stronger propensity towards σ-donation of cyclic (alkyl)(amino) carbenes (CAAC)[25,26] has been highlighted both in catalytic applications[27] and in pioneering on-surface reactivity studies by Johnson and co-workers,[28] but little is known about the fundamental behavior of such entities on metal surfaces.[29] A profound understanding of the binding modes, the conformation, and the supramolecular assembly of CAACs on surfaces will offer a springboard for the development of tailor-made systems for catalysis[23] and advanced materials.[30] Kwon *et al.* reported that the ratio of the equatorial and axial chair conformers in cyclohexanethiol is influenced by the molecule concentrations on metal surface.[31] Beyond that, cyclohexyl as a side group of a CAAC should give rise to some promising tunable self-assemblies on the surfaces.[32,33]

Therefore, as outlined in Scheme 1a, we devised a straightforward synthetic route to access cyCAAC • CO_2, which upon heating under vacuum liberated the free carbene without potential surface contaminants.[29] The corresponding hydrochloride salt (cyCAAC • HCl) — obtained according to the procedure by Bertrand and co-workers —[34] was deprotonated in Et_2O with lithium diisopropylamide (LDA). Solvent exchange and filtration allowed the removal of insoluble inorganic byproducts, then the cyCAAC was treated with carbon dioxide to generate the zwitterionic adduct cyCAAC • CO_2, which was isolated as a white powder. Fortunately, a specimen suitable for X-ray analysis could be crystallized by slow evaporation from a CH_2Cl_2/THF mixture at -18°C (Scheme 1b).[35] The compound crystallized with one water molecule in the asymmetric unit, which is involved trough OH···O hydrogen bonds interactions in the formation of a dimeric structure. These dimeric units form a linear chain along the a-axis trough additional CH···O interactions. No relevant π···π or CH···π interactions were observed in the packing diagram of cyCAAC • CO_2 compound (see Scheme 1b - right).

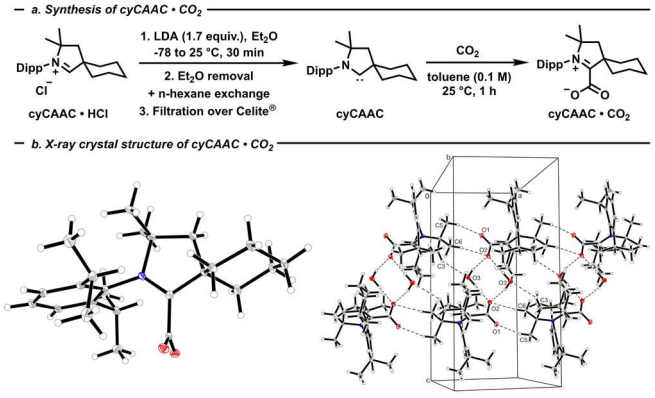

Scheme 1. a. Synthesis of cyCAAC • wCO_2. Dipp = 2,6 di*iso*propylphenyl. **b**. X-ray crystal structure of cyCAAC • CO_2 and crystal packing. Thermal ellipsoids are shown at 30% probability level.

Herein, we report an in-depth study of the binding mode, conformational switching and their influence on the self-assembly of cyCAAC on Au (111), Ag (111) and Cu (111) surfaces, at coverages from sub-monolayer to monolayer saturation.[36] One monolayer coverage (ML) is defined as the amount of cyCAAC molecules that fully covers the surface area, and in the case of cyCAAC on Au (111) 1 ML corresponds to 0.96 molecule/nm^2. In particular, we will prove that conformational changes can determine molecular self-assembly on the Au (111) substrate, where surface reconstruction yields multiple regions with various electronic density of states. In addition, a powerful experimental method to reversibly switch[37] the conformations and their accompanying self-assembly of cyCAAC is displayed. To learn the importance of cyCAAC-surface interactions on monolayer structures,[38] Ag (111) and Cu (111) are also chosen as substrates. The ballbot-like species of the cyCAAC on Au (111) does not appear on Ag (111) and Cu (111). On the Ag (111) surface, only close-packed dimer phase is observed. This phase is coverage independent, i.e. both low and high coverage samples manifest the same dimer phase. For the Cu (111) surface, the cyCAAC bound Cu atom is still fixed within the first layer, which is similar to the case on Ag (111) but different from the ballbot-like species on Au (111). Well-separated stripes at 0.6 monolayer coverage constitute an ideal template for synthesizing some multifunctional cyCAAC-based complexes.

Results and Discussion

We first tested cyCAAC on a herringbone reconstructed Au (111) surface and studied the restructuring of the molecular self-assembly. This well-known surface exhibits alternating fcc and hcp areas separated by domain walls and thus has remarkably repeated adsorption potential regions for adsorbates.[39] After deposition at room temperature (300 K) with a base pressure of 4.0 × 10^{-10} mbar and cooling to 78 K for STM analysis, the growth of cyCAAC preferentially starts at the fcc regions with a triangular close-packed phase (labeled as trimer phase) at low coverage (0.4 ML), as seen in Figure 1a. The preferential separate adsorption is due to the lower adsorption energy than those of the hcp regions.[40] The enlarged STM images (Figures 1b and SII-1b) illustrate that this phase is constructed by two kinds of chiral trimers, i. e, *R* and *L* units as shown in Figure 1c. Each unit involves three cyCAAC molecules with different molecular arrangement. Although trimers in every continuously fcc region manifest identical chirality, Figure SII-1b proves that neighbor fcc regions have random chirality. The absence of long-range chirality recognition here eliminates the origin of local dipole accumulation when explaining the below self-assembly transitions.[41]

Further increasing the coverage gives rise to occupation of hcp region with chainlike structure, see 0.6 ML in Figure 1d. Due to alternative configuration in each chain, we labeled the new molecular arrangement in Figure 1f as a dimer phase. Figure SII-2 reveals that the internal distance within the triangular unit is 1.02±0.05 nm while interval distance between two neighbor trimer units is 1.94±0.07 nm. The internal distance within the dimer unit is 0.95±0.05 nm while interval distances between two neighbor dimer units are 1.62±0.06 nm along the chain and 1.22±0.06 nm perpendicular to the chain, respectively. Therefore, the cyCAAC surface mobility is directly proved by changing from the trimer to the dimer phase, as distances between molecules have changed.

Interestingly, statistical analysis based on intermediate coverage sample similar to Figure 1d reveals that the trimer phase in fcc domains will spontaneously change to a dimer phase once one of the two adjacent hcp regions is filled by cyCAAC. This conclusion can be further verified on the 1 ML coverage sample where only the dimer phase can be found on the whole surface. As indicated by the light blue dashed lines in Figure 1e, all previous trimer phases on fcc domain have been completely transferred to the dimer phase. Notably, such transition can be switched back by reducing molecular coverage via annealing process, which will be discussed in the following.

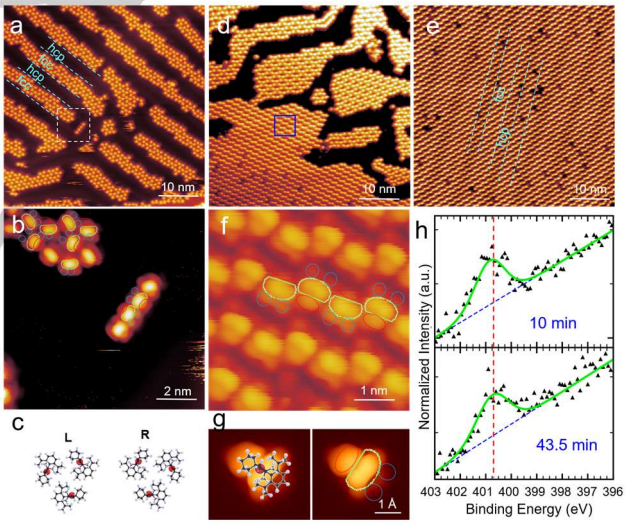

Figure 1. cyCAAC on a √3 × 22 herringbone Au (111) surface. The molecular evaporation temperature is 80 °C while the evaporation time in (a), (d) and (e) are 3 min, 6 min and 10 min, respectively. (a) 0.4 ML sample where only fcc regions were occupied. (b) Zoom in the white dash square area in (a) shows high resolution STM topography of trimers. (c) The top view of the models for R and L-chiral trimers. (d) 0.6 ML sample where some hcp regions were occupied. (e) 1.0 ML sample where only dimer phase was discovered. (f) Zoom in the blue square area in (d). The superimposed red ellipses display the cyclohexyl side groups. (g) STM simulation based on cyCAAC molecular framework on Au (111). (h) N1s XPS spectra of cyCAAC on Au (111) surface with different deposition time.

Our observation of the large-scale self-assembly switching has immediately raised one important question concerning the intrinsic mechanism. Recently, Bakker *et al.* reported on the DiMeCAAC on metal surfaces and showed no self-assembly.[29] Given that the only difference between the DiMeCAAC and cyCAAC comes from the new cyclohexyl side group, the

interesting self-assembly evolution herein reported should be attributed to the conformational switching in the flexible 6-membered aliphatic ring. To prove the Dipp group sides in these two CAACs have identical chemical state, XPS measurements in Figure 1h were performed to check the N1s signal in cyCAAC on the Au (111) surface. During XPS measurements, the absence of signal in O 1s region indicates the successful decarboxylation during deposition, see Figure SII-3. One peak is found in the N 1s region at 400.79 eV, which can be attributed to the surface-bound cyCAAC and manifests the same value as the previously reported DiMeCAAC.[29] Consequently, the wingtip Dipp group in cyCAAC and DiMeCAAC should have similar chemical environment and same contribution to the molecular assembly.

Actually, the close-up topographies in Figures 1b and 1f show that the individual cyCAAC molecule is imaged as a bright semicircle with one or two ellipse shadows on each side, and among them, the single dim ellipse feature (red ellipse in Figure 1f) corresponds to the cyclohexyl side group while the two ellipse shadows (blue circles in Figure 1f) are the methyl parts, which can be easily inferred from the STM simulation in Figure 1g. The STM topography of cyclohexyl was caused by a convolution of the electron wave functions of the tip and the sample.[42] It is difficult to resolve chair conformer only based on imaging.[40] Besides, fluctional motion or rotation at 78 K could cause the structureless features as well. To determine the detail molecular isomers in the trimer/dimer phases and expose their underlying influence in self-assembly transitions,[13] we have adopted DFT calculations to prove that conformational switching is the direct reason.

Due to conformational isomerism of the cyclohexyl fragment, the equatorial and axial chair conformers are expected according to the orientations of cyclohexyl with respect to the Dipp plane. Skew-boat conformers are excluded due to the high energy compared to that in chair conformers.[43] In fact, an upright binding mode with a strong cyCAAC-metal bond is expected and confirmed by DFT simulations for both chair conformers, see Figures 2a and 2b. Actually, the same N 1s peak positions from cyCAAC and DiMeCAAC[29] indicate identical upright binding mode since different binding modes should change peak position rapidly[32]. CyCAAC with the Dipp group perpendicular to the CAAC ring and parallel to the surface can be easily found and is also consistent with the previous DiMeCAAC work.[29]

To learn the observed phase transition, DFT simulations based on the trimer and dimer phases with different conformers were performed. Based on the upright standing model of the isomers, the adsorption configurations of the trimer and dimer phases are constructed. For the trimer phase, DFT calculations reveal that the adsorption energy of the axial chair conformers is 0.12 eV lower than the equatorial ones, as shown in Table SII-1. Thus, the trimer consisting of axial chair conformers is more stable, while the dimer consisting of equatorial chair conformers is more stable. Therefore, a conformational transition from axial to equatorial happens if the trimer phase is transferred to the dimer phase.

We have calculated and compared the adsorption energies of cyCAAC molecules on the Au (111) surface of the trimer and dimer phases, as summarized in Figure 2e. The adsorption energy was calculated in two ways as follows:

$$E_{ads}^{1} = (E_{tot} - E_{ad} - E_{bare})/N$$
$$E_{ads}^{2} = (E_{tot} - E_{ad} - E_{bare})/S$$

where the E_{tot} (E_{bare}) is the energy of the substrate with (without) adsorbate and E_{ad} is the energy of the isolated adsorbate species. N is the number of the molecules in the unit cell and S is the area of the unit cell. Hence, a negative E_{ads} indicates stable adsorption whereas a positive value indicates unstable adsorption, with a more negative value indicating more favorable adsorption. Since the adsorption structure of molecules at low (high) coverage is mainly determined by the adsorption energy per molecule (per area), the E_{ads}^{1} (E_{ads}^{2}) is used to evaluate the stability of the adsorption structure at low (high) coverage.[44]

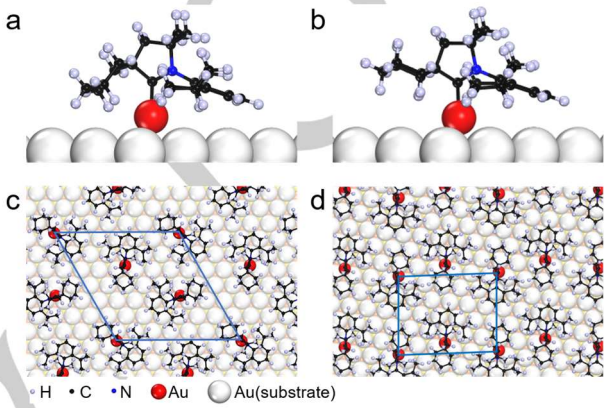

e

Adsorption phase	E_{ads}^{1} eV/molecule	E_{ads}^{2} eV/Å^2
Trimer	-4.06	-0.033
Dimer	-3.98	-0.038

Figure 2. The optimized structures of the trimer and dimer phases. (a, b) Side views of the DFT-optimized geometry of the upstanding binding mode of cyCAAC on Au (111). Ring-flip of cyclohexyl in cyCAAC results in two chair conformations, i.e. axial (a) and equatorial (b) isomer, on Au (111). (c) The top view of the trimer phase formed by axial chair conformer. (d) The top view of the dimer phase formed by the equatorial chair conformer. The blue lines indicate the unit cells of the trimer phase in (c) and dimer phase in (d). The light purple, black and blue balls represent H, C and N atoms in cyCAAC molecule. The red and white balls represent Au adatoms bound to cyCAAC molecules and Au atoms on substrate, respectively. (e) Adsorption energies of the trimer and dimer phases on Au (111) surface.

The E_{ads}^{1} of the trimer and dimer phases are -4.06 eV/molecule and -3.98 eV/molecule, respectively. While the E_{ads}^{2} of the trimer and dimer phases are -0.033 eV/Å^2 and -0.038 eV/Å^2, respectively. Thus, at low coverage, the trimer phase is more stable. As the coverage increases, the dimer phase becomes the most stable adsorption configuration. Such transition also coincides well with previous literatures, i. e. the equatorial conformer is more favorable at high concentrations.[45]

Subsequently we prolonged the deposition time to 43.5 minutes to create multi-layer sample. Surprisingly, only 1 ML rather than multi-layer structure was found based on the STM images and a quantitative analysis of the N1s peak in XPS measurement, see Figure 1h. An empty molecular source in evaporator can be excluded from the subsequent consistent relationship between coverage and deposition conditions, i.e. 1 ML covered sample always can be achieved when deposition time is 10 minutes. Therefore, the interlayer interaction between cyCAAC is relative weak. Further molecules cannot be deposited on the surface at 300 K once the metal surface was saturated by 1 ML molecules.

To reversibly switch the molecular conformers and self-assembly, we reduce the coverage via thermal annealing

induced desorption without any molecular decomposition. As we should notice, the exact desorption process of carbene on the surface might involve complex pathways during annealing procedure, which provides additional energy for the surface and thus destructs any residue evidences like potential adatom on the surface. Besides, it is difficult to analyze desorption fragments, as the concentration was always too low for analysis by mass spectrometry. Annealing a full monolayer sample with dimer phase in Figure 1e resulted in the reappearance of trimer phase when parts of the hcp regions are bare, see Figures 3a-3c. During the heating process, molecules at the hcp regions first desorb. Finally, the molecular arrangements at the fcc region will transfer back to the previous trimer phase again when both adjacent two hcp regions are bare, see Figure 3b. The internal distance within the new trimer phase unit and interval distance between two neighbor trimer units are the same as those measured in initial low coverage case in Figure SII-2.

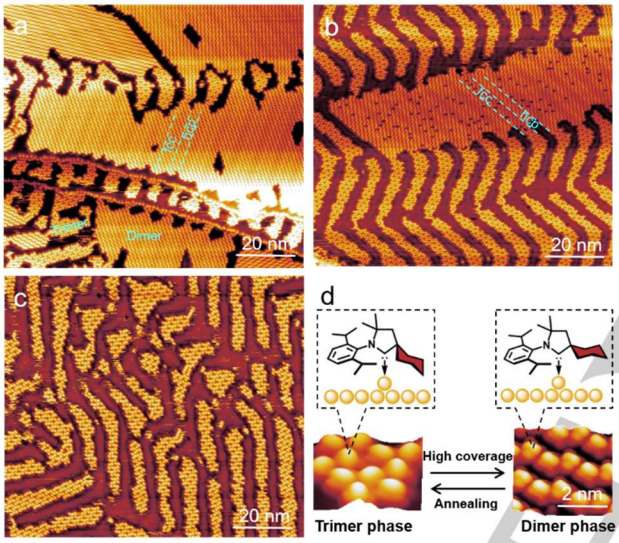

Figure 3. Gradually annealing sample from (a) to (c). Parameters: (a) 470 K for 15 min. (b) 490 K for 15 min. (c) 500 K for 15 min. (d) Reversible switching of cyCAAC conformers and their self-assembly structures, i.e. axial chair conformer in trimer phase while equatorial chair conformer in dimer phase, via tuning molecular coverage.

Simultaneously, monomers with uniform molecular topography are presented within the self-assembly after each annealing process, in contrast to a previously investigated system of Pt(II) complexes, which involves scission of a C-N bond at the head of the complexes.[46] The cyCAAC covered Au (111) sample will become a completely clean surface when annealing the sample at 520 K for 15 min. Thus, such molecular self-assembly switching, especially in fcc regions, can be consistently achieved back and forth for many times, as illustrated in Figure 3d.

In order to uncover how the adsorption behavior of cyCAAC changes with different metal substrates, we also deposited molecules on Ag (111) and Cu (111) surfaces. For molecules on Ag (111) surface, only the dimer phase structure was observed on both low and high coverage samples, see Figure SII-4. The cyCAAC-Ag distance (Table SII-4) indicates a different binding mode from ball-bot like species, i.e. Ag atom cannot be fully extracted from the surface due to the lower adsorption height of the Ag atom bound to cyCAAC molecule comparing with Ag adatom. However, large scale STM topography of a Cu (111) surface covered by disordered assembly was depicted in Figure SII-5. Upon annealing at 400 K, regular highly ordered chain structures separated by regular spacing come into sight in Figure 4.

Similar to 1 ML sample on Au (111) surface, a close-packed dimer phase chains occupied the Cu (111) surface in Figure 4a. Figures 4b and 4d show high resolution images in the chains, demonstrating a clear dimer phase on the surface. Line profile along the red line in Figure 4b reveals the same internal distance (d=1.2 nm) as the one on Au (111). When reducing the coverage to 0.6 ML, we get a surprisingly ordered structure, i.e. large-scale areas of stripes separated by a constant distance at 3.7 nm. The internal distance between chains within the stripes is the same as that in 1 ML surface, see Figure 4e. The stripes contain two or three chains. A statistical analysis of the number, based on several hundreds of stripes obtained from STM images, determined that the amounts of the two-chain and three-chain configurations are 95% and 5%, respectively. Notably, we have detected a strong correlation between the interval distance (D) between the stripes and internal value (d) between the chains within the stripe. A Gaussian fit of the statistical results of D summarized in Figure 4f shows a value of 3.7±0.3 nm, which is three times of internal distance d.

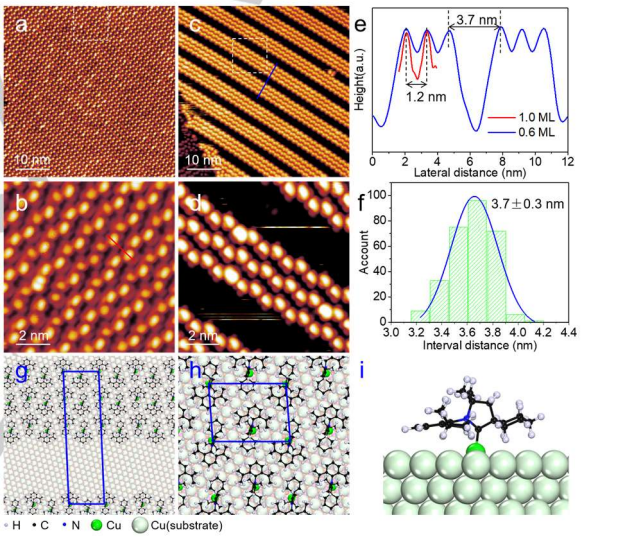

Figure 4. (a-d) Constant-current STM images of different coverage cyCAAC molecules on Cu (111) after annealing at 400 K. (a, b) close packed structure at 1.0 ML (Density: 1.06 molecule/nm^2); (c, d) stripe structure at 0.6 ML. (b) and (d) correspond to the white squares showed in (a) and (c). (e) Line profiles along red and blue lines depicted in (b) and (c). (f) Statistical analysis of interval distance between adjacent stripes. (g)-(i) The optimized structures of the stripe and close packed dimer phases on Cu (111). (g) The top view of the stripe structure. (h) The top view of the close packed structure. The blue lines indicate the unit cells of the stripe and close packed structures. (i) The side view of the adsorption geometry of the equatorial chair cyCAAC molecule on Cu (111). The light purple, black and blue balls represent H, C and N atoms in cyCAAC molecules. The green and light green balls represent Cu atoms bound to cyCAAC molecules and Cu atoms on substrate, respectively.

To understand the discovered separated stripes on 0.6 ML sample, DFT simulations were performed to investigate the molecular structures of the stripe and the close packed structures in Figures 4b and 4d. The optimized geometries of the stripe and the close packed arrangements of cyCAAC molecules adsorbed on Cu (111) surface were depicted in Figures 4g and 4h. The distance between the molecule chains is calculated to be 11.7 Å, which is in good agreement with the experimental observations. Different from the cyCAAC molecules on Au (111) surface, where the molecules bind to the Au adatoms on the substrate, the Cu atom covalently connected to cyCAAC molecule is still in the first layer of the substrate, as shown in

Figure 4i. The adsorption energies of these two structures are calculated and summarized in Table SII-3. The E_{ads}[1] of the separated stripe is -2.57 eV/molecule, being more stable than the close packed structures. Thus, at low coverage, cyCAAC molecules prefer to form the separated stripes.

Conclusion

In conclusion, the binding mode, surface geometry and reversible self-assembly of cyCAAC on metal surfaces were studied by LT-STM, XPS and DFT calculations. The large-scale transitions of self-assembly on reconstructed Au (111) surface have been proved to be caused by the conformational switching in the flexible 6-membered aliphatic ring in cyCAAC. In the sub-monolayer case, cyCAAC with only axial chair conformer formed a trimer phase on the fcc regions. However, when increasing the coverage, cyCAAC with only equatorial chair conformer emerged into a dimer phase and covered the whole surface on 1 ML sample. The equatorial chair conformer can turn back to axial chair conformer when reducing molecular coverage through annealing. Therefore, the conformational switching, including their self-assembly, of cyCAAC has been reversibly performed here. Furthermore, self-assembly of cyCAAC on other metal surfaces, especially on Cu (111) surface, has manifested highly ordered nanopatterns. A coverage independent dimer phase was observed on Ag (111) surface. While for Cu(111), the regular bare areas on the 0.6 ML sample provide enough space for reactive adsorption. We are confident that such regular structures, especially the controllable ratio of surface to volume caused by conformational switching, will be of great importance in constructing patterned supramolecular assembly carbene structures[37,47,48] for future applications in catalysis and beyond.[8,23]

Acknowledgements

The authors acknowledge financial support from the Deutsche Forschungsgemeinschaft (DFG) (TRR 61, SFB 858, FU 299/18-1), Strategic Priority Research Program of Chinese Academy of Sciences, (Grant No. XDB36000000, No. XDB30000000), the National Natural Science Foundation of China (No. 61888102), and CAS Project for Young Scientists in Basic Research (YSBR-003). We also thank Elena Kolodzeiski and Saeed Amirjalayer (both Westfälische Wilhelms-Universität) for theory discussion.

Keywords: CAAC • reversible self-assembly • surfaces • scanning probe microscopy• conformational switching

[1] A. J. Arduengo, R. L. Harlow, M. Kline, *J. Am. Chem. Soc.* **1991**, *113*, 361–363.

[2] G. C. Fortman, S. P. Nolan, *Chem. Soc. Rev.* **2011**, *40*, 5151–5169.

[3] Q. Zhao, G. Meng, S. P. Nolan, M. Szostak, *Chem. Rev.* **2020**, *120*, 1981–2048.

[4] G. C. Vougioukalakis, R. H. Grubbs, *Chem. Rev.* **2010**, *110*, 1746–1787.

[5] V. Nesterov, D. Reiter, P. Bag, P. Frisch, R. Holzner, A. Porzelt, S. Inoue, *Chem. Rev.* **2018**, *118*, 9678–9842.

[6] C. M. Crudden, D. P. Allen, *Coord. Chem. Rev.* **2004**, *248*, 2247–2273.

[7] M. N. Hopkinson, C. Richter, M. Schedler, F. Glorius, *Nature* **2014**, *510*, 485–496.

[8] P. Bellotti, M. Koy, M. N. Hopkinson, F. Glorius, *Nat. Rev. Chem.* **2021**, *5*, 711–725.

[9] C. M. Crudden, J. H. Horton, I. I. Ebralidze, O. V. Zenkina, A. B. McLean, B. Drevniok, Z. She, H. B. Kraatz, N. J. Mosey, T. Seki, E. C. Keske, J. D. Leake, A. Rousina-Webb, G. Wu, *Nat. Chem.* **2014**, *6*, 409–414.

[10] J. Ren, M. Freitag, C. Schwermann, A. Bakker, S. Amirjalayer, A. Rühling, H.-Y. Gao, N. L. Doltsinis, F. Glorius, H. Fuchs, *Nano Lett.* **2020**, *20*, 5922–5928.

[11] M. Franz, S. Chandola, M. Koy, R. Zielinski, A. Aldahhak, M. Das, M. Freitag, U. Gerstmann, D. Liebig, A. K. Hoffmann, M. Rosin, W. G. Schmidt, C. Hogan, F. Glorius, N. Esser, M. Dähne, *Nat. Chem.* **2021**, *13*, 828–835.

[12] A. V Zhukhovitskiy, M. G. Mavros, T. Van Voorhis, J. A. Johnson, *J. Am. Chem. Soc.* **2013**, *135*, 7418–7421.

[13] A. Inayeh, R. R. K. Groome, I. Singh, A. J. Veinot, F. C. de Lima, R. H. Miwa, C. M. Crudden, A. B. McLean, *Nat. Commun.* **2021**, *12*, 4034.

[14] M. J. MacLeod, J. A. Johnson, *J. Am. Chem. Soc.* **2015**, *137*, 7974–7977.

[15] M. J. MacLeod, A. J. Goodman, H.-Z. Ye, H. V.-T. Nguyen, T. Van Voorhis, J. A. Johnson, *Nat. Chem.* **2019**, *11*, 57–63.

[16] R. Ye, A. V Zhukhovitskiy, R. V Kazantsev, S. C. Fakra, B. B. Wickemeyer, F. D. Toste, G. A. Somorjai, *J. Am. Chem. Soc.* **2018**, *140*, 4144–4149.

[17] R. W. Y. Man, C.-H. Li, M. W. A. MacLean, O. V Zenkina, M. T. Zamora, L. N. Saunders, A. Rousina-Webb, M. Nambo, C. M. Crudden, *J. Am. Chem. Soc.* **2018**, *140*, 1576–1579.

[18] M. R. Narouz, K. M. Osten, P. J. Unsworth, R. W. Y. Man, K. Salorinne, S. Takano, R. Tomihara, S. Kaappa, S. Malola, C.-T. Dinh, J. D. Padmos, K. Ayoo, P. J. Garrett, M. Nambo, J. H. Horton, E. H. Sargent, H. Häkkinen, T. Tsukuda, C. M. Crudden, *Nat. Chem.* **2019**, *11*, 419–425.

[19] K. V. S. Ranganath, J. Kloesges, A. H. Schäfer, F. Glorius, *Angew. Chem. Int. Ed.* **2010**, *49*, 7786–7789; *Angew. Chem.* **2010**, *122*, 7952–7956.

[20] J. B. Ernst, C. Schwermann, G. Yokota, M. Tada, S. Muratsugu, N. L. Doltsinis, F. Glorius, *J. Am. Chem. Soc.* **2017**, *139*, 9144–9147.

[21] P. Godbold, G. Johnson, A. D. Obi, R. Brown, S. Hwang, J. Robert J. Gilliard, S. Zhang, *J. Am. Chem. Soc.* **2021**, *143*, 2644–2648.

[22] C. A. Smith, M. R. Narouz, P. A. Lummis, I. Singh, A. Nazemi, C. H. Li, C. M. Crudden, *Chem. Rev.* **2019**, *119*, 4986–5056.

[23] M. Koy, P. Bellotti, M. Das, F. Glorius, *Nat. Catal.* **2021**, *4*, 352–363.

[24] A. V. Zhukhovitskiy, M. J. MacLeod, J. A. Johnson, *Chem. Rev.* **2015**, *115*, 11503–11532.

[25] M. Soleilhavoup, G. Bertrand, *Acc. Chem. Res.* **2015**, *48*, 256–266.

[26] M. Melaimi, R. Jazzar, M. Soleilhavoup, G. Bertrand, *Angew. Chem. Int. Ed.* **2017**, *56*, 10046–10068; *Angew. Chem.* **2017**, *129*, 10180–10203.

[27] a) R. Jazzar, M. Soleilhavoup, G. Bertrand, *Chem. Rev.* **2020**, *120*, 4141–4168; b) V. Lavallo, Y. Canac, A. DeHope, B. Donnadieu, G. Bertrand, *Angew. Chem. Int. Ed.* **2005**, *44*, 7236-7239; *Angew. Chem.* **2005**, *117*, 7402-7405.

[28] A. V Zhukhovitskiy, M. G. Mavros, K. T. Queeney, T. Wu, T. Van Voorhis, J. A. Johnson, *J. Am. Chem. Soc.* **2016**, *138*, 8639–8652.

[29] A. Bakker, M. Freitag, E. Kolodzeiski, P. Bellotti, A. Timmer, J. Ren, B. Schulze Lammers, D. Moock, H. W. Roesky, H. Mönig, S. Amirjalayer, H. Fuchs, F. Glorius, *Angew. Chem. Int. Ed.* **2020**, *59*, 13643–13646; *Angew. Chem.* **2020**, *132*, 13745–13749.

[30] S. Dery, P. Bellotti, T. Ben-Tzvi, M. Freitag, T. Shahar, A. Cossaro, A. Verdini, L. Floreano, F. Glorius, E. Gross, *Langmuir* **2021**, *37*, 10029–10035.

[31] C. K. Kwon, M. S. Kim, K. Kim, *J. Raman Spectrosc.* **1989**, *20*, 575–580.

[32] A. Bakker, A. Timmer, E. Kolodzeiski, M. Freitag, H. Y. Gao, H. Mönig, S. Amirjalayer, F. Glorius, H. Fuchs, *J. Am. Chem. Soc.* **2018**, *140*, 11889–11892.

[33] C. R. Larrea, C. J. Baddeley, M. R. Narouz, N. J. Mosey, J. H. Horton, C. M. Crudden, *ChemPhysChem* **2017**, *18*, 3536–3539.

[34] R. Jazzar, R. D. Dewhurst, J.-B. Bourg, B. Donnadieu, Y. Canac, G. Bertrand, *Angew. Chem. Int. Ed.* **2007**, *46*, 2899–2902; *Angew. Chem.* **2007**, *119*, 2957–2960.

[35] CCDC 1944014 contains the supplementary crystallographic data for this paper. These data can be obtained free of charge from The Cambridge Crystallographic Data Centre.

[36] G. Wang, A. Rühling, S. Amirjalayer, M. Knor, J. B. Ernst, C. Richter, H.-J. Gao, A. Timmer, H.-Y. Gao, N. L. Doltsinis, F. Glorius, H. Fuchs, *Nat. Chem.* **2017**, *9*, 152–156.

[37] D. T. Nguyen, M. Freitag, C. Gutheil, K. Sotthewes, B. J. Tyler, M. Böckmann, M. Das, F. Schlüter, N. L. Doltsinis, H. F. Arlinghaus, B. J. Ravoo, F. Glorius, *Angew. Chem. Int. Ed.* **2020**, *59*, 13651–13656; *Angew. Chem.* **2020**, *132*, 13754–13759.

[38] J. Ren, E. Larkin, C. Delaney, Y. Song, X. Jin, S. Amirjalayer, A. Bakker, S. Du, H. Gao, Y.-Y. Zhang, S. M. Draper, H. Fuchs, *Chem. Commun.* **2018**, *54*, 9305–9308.

[39] L. Gao, W. Ji, Y. B. Hu, Z. H. Cheng, Z. T. Deng, Q. Liu, N. Jiang, X. Lin, W. Guo, S. X. Du, W. A. Hofer, X. C. Xie, H.-J. Gao, *Phys. Rev. Lett.* **2007**, *99*, 106402.

[40] J. Ren, Y. Wang, J. Zhao, S. Tan, H. Petek, *J. Am. Chem. Soc.* **2019**, *141*, 4438–4444.

[41] H. Kong, Y. Qian, X. Liu, X. Wan, S. Amirjalayer, H. Fuchs, *Angew. Chem. Int. Ed.* **2020**, *59*, 182–186; *Angew. Chem.* **2020**, *132*, 188–192.

[42] J. Ren, H. Guo, J. Pan, Y.-F. Zhang, Y. Yang, X. Wu, S. Du, M. Ouyang, H.-J. Gao, *Phys. Rev. Lett.* **2017**, *119*, 176806.

[43] H. Kang, J. Noh, E. O. Ganbold, D. Uuriintuya, M. S. Gong, J. J. Oh, S. W. Joo, *J. Colloid Interface Sci.* **2009**, *336*, 648–653.

[44] H. Cun, Y. Wang, S. Du, L. Zhang, L. Zhang, B. Yang, X. He, Y. Wang, X. Zhu, Q. Yuan, Y.-P. Zhao, M. Ouyang, W. A. Hofer, S. J. Pennycook, H. Gao, *Nano Lett.* **2012**, *12*, 1229–1234.

[45] S. W. Joo, H. Chung, K. Kim, J. Noh, *Surf. Sci.* **2007**, *601*, 3196–3201.

[46] J. Ren, M. Cnudde, D. Brünink, S. Buss, C. G. Daniliuc, L. Liu, H. Fuchs, C. A. Strassert, H.-Y. Gao, N. L. Doltsinis, *Angew. Chem. Int. Ed.* **2019**, *58*, 15396–15400; *Angew. Chem.* **2019**, *131*, 15542–15546.

[47] D. T. Nguyen, M. Freitag, M. Körsgen, S. Lamping, A. Rühling, A. H. Schäfer, M. H. Siekman, H. F. Arlinghaus, W. G. van der Wiel, F. Glorius, B. J. Ravoo, *Angew. Chem. Int. Ed.* **2018**, *57*, 11465–11469; *Angew. Chem.* **2018**, *130,* 11637–11641.

[48] Z. She, M. R. Narouz, C. A. Smith, A. MacLean, H.-P. Loock, H.-B. Kraatz, C. M. Crudden, *Chem. Commun.* **2020**, *56*, 1275–1278.

10.1002/anie.202115104

Entry for the Table of Contents

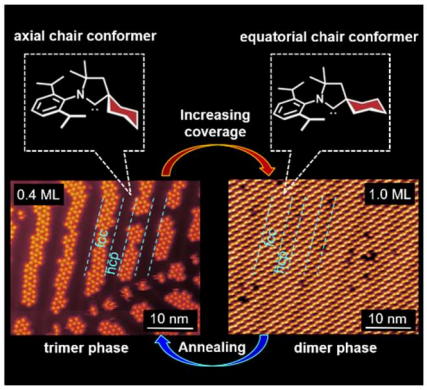

The reversible self-assembly of N-heterocyclic carbene mediated by conformational switching can be tuned via controllable experimental conditions, leaving behind different largely ordered structures. Such method provides a new alternative and convenient method to influence the self-assembled structure of NHC-metal monolayers, a still missing but essential tool towards catalytic applications.

Institute and/or researcher Twitter usernames:

@GloriusGroup; @94peter; @matze_Freitag; @GloriusFrank